PHILOSOPHICAL TRANSACTIONS OF THE ROYAL SOCIETY A MATHEMATICAL, PHYSICAL & ENGINEERING SCIENCES

Laboratory Models of Circulation in Shallow Seas

J. A. Whitehead

Phil. Trans. R. Soc. Lond. A 1981 **302**, 583-595
doi: 10.1098/rsta.1981.0184

Phil. Trans. R. Soc. Lond. A **302**, 583–595 (1981)
Printed in Great Britain

Laboratory models of circulation in shallow seas

By J. A. Whitehead, Jr
Woods Hole Oceanographic Institution, Woods Hole, Massachusetts 02543, *U.S.A.*

[Plate 1]

Three laboratory experiments are described. The first was made to observe the flow field of circulation in a model given by Stommel & Leetmaa (1972). The experiment consisted of a very shallow (1 or 2 cm deep) annulus with an inner heated wall of radius 25 cm and a cooled outer wall of radius 57 cm, all mounted on a turntable. When the Ekman number was large the flow was steady and resembled the solutions for a non-rotating estuary given by Hansen & Rattray (1965), but when the Ekman number was small the flow became time-dependent. Values of shear and stratification obtained from theory indicate that the flowing water probably underwent baroclinic instability. It appears that such instability may develop on real shelves.

The second experiment consisted of a shallow sea of constant depth bounded by a deep ocean through a uniformly sloping continental rise. The experiment is cooled from above and there is a region that exhibits sinking convection cells, which form the coldest water. This water then spills off the right-hand side of the shallow sea (looking downstream for counterclockwise rotation) and forms bottom water in the deep experimental ocean.

The third experiment is a rotating version of the dam-break problem in which a density current is generated after a barrier has been removed. The rotation causes the current to lean against the right-hand wall (looking downstream for counterclockwise rotation) and turbulent eddies are detrained to the side rather than vertically.

1. The Stommel–Leetmaa shelf model

Although there have been many theoretical studies of the dynamics of the oceanic waters on continental-shelf regions, few have been concerned with theories of the general circulation in such regions. One of the first attempts appears to have been an idealized model by Stommel & Leetmaa (1972), which concerns the flows on an infinitely long, straight, constant-depth shelf, subjected to wind stress from above and to fresh water run-off from the continental side. The effects of friction, diffusion, and cross-shelf advection were retained in the governing equations, which were derived by the use of an expansion procedure based on the fact that the ratio of shelf depth to width is very small. Given values of the top wind stress, fresh water run-off, depth and width of the shelf, and 'eddy' properties of the water's viscosity, diffusivity and alongshore pressure gradient, they predicted the cross-shelf density gradient and alongshelf velocity. The numbers believed to be appropriate for the Mid-Atlantic Bight were used to assess the appropriateness of the model to the real shelf, as discussed subsequently by Csanady (1976), Scott & Csanady (1976) and others.

Here I do not continue to discuss applications of this theory to real shelves, but instead observe features of this model through observations of flows in a very shallow annulus experiment in the laboratory. I desired to see if any additional boundary layers or instabilities could be observed, or whether the flow otherwise did not behave as predicted. The dynamics of the experiment differ from the above theories because there is a heat flux rather than a water flux and there are rigid boundary conditions at the top. Hence a brief reformulation will be given.

Formulation of the problem

The model consists of a layer of fluid of constant depth d, breadth L, infinitely long, and subject to a lateral temperature gradient $\partial T/\partial x$ across its breadth as a model of lateral density gradient. The system is rotating at rate $\frac{1}{2}f$ in a field of gravity g. The viscosity ν of the fluid is constant, as is the thermal diffusivity κ and the coefficient of expansion α. The Boussinesq equations will be presented in a dimensionless form by using d as the vertical length scale, L as the horizontal length scale, fd as the horizontal velocity scale, fd^2/L as the vertical velocity scale, $\rho f^2 d$ as the pressure scale (ρ is average density), and by representing the temperature as

$$T' = (x + dT)\,\partial T/\partial x, \tag{1}$$

so T is the dimensionless temperature correction to a linear temperature distribution in the x-direction (across the shelf).

If $d \ll L$ vertical velocities will be much smaller than horizontal ones except near the lateral edges. The Boussinesq equations with all terms of order d/L neglected are

$$-v = -p_x + Eu_{zz}, \quad u = Ev_{zz}, \tag{2 a, b}$$

$$p_z = -Sx, \quad u = PT_{zz}, \tag{2 c, d}$$

where a subscript denotes partial differentiation and

$$S \equiv (g\alpha/f^2)\,\partial T/\partial x, \quad P \equiv \kappa/fd^2 \quad \text{and} \quad E \equiv \nu/fd^2.$$

The simplest solutions are antisymmetrical above and below the plane $z = 0$. Pressure at any height z can be found by integrating $(2c)$. The x-derivative of pressure at this value of z is

$$p_x = -Sz + C, \tag{3}$$

where C is the lateral pressure gradient at $z = 0$.

The left side of equation $(2d)$ is a lateral advection of heat. The right-hand side is the 'short-circuiting' effect first noted by Taylor (1953) for problems where there is advection in one direction and conduction principally in another direction with smaller length-scale.

To model 'wind stress', it will be assumed that the top and bottom boundaries move with equal and opposite velocities. In addition there will be no vertical heat transfer through the boundaries, and hence the boundary conditions are

$$u = \pm U, \quad v = \pm V \quad \text{and} \quad \partial T/\partial z = 0 \quad \text{at} \quad z = \pm \tfrac{1}{2}. \tag{4}$$

Solutions have the form

$$u = (-\tfrac{1}{2}S - V)\,g_1(z) + Ug_2(z), \tag{5a}$$

$$v = +(\tfrac{1}{2}S + V)\,g_2(z) + Ug_1(z) - Sz, \tag{5b}$$

$$T = (\tfrac{1}{2}S + V)\frac{E}{P}\,g_2(z) + U\frac{E}{P}\,g_1(z) - \frac{\beta E z}{P(\cosh\beta - \cos\beta)}\,(\tfrac{1}{2}S + V + U)\sinh\beta + (\tfrac{1}{2}S + V - U)\sin\beta, \tag{5c}$$

where

$$\beta = (2E)^{-\frac{1}{2}}, \tag{6a}$$

$$g_1(z) = [\sinh\beta(z+\tfrac{1}{2})\sin\beta(z-\tfrac{1}{2}) - \sinh\beta(z-\tfrac{1}{2})\sin\beta(z+\tfrac{1}{2})]/(\cosh\beta - \cos\beta), \tag{6b}$$

$$g_2(z) = [\cosh\beta(z+\tfrac{1}{2})\cos\beta(z-\tfrac{1}{2}) - \cosh\beta(z-\tfrac{1}{2})\cos\beta(z+\tfrac{1}{2})]/(\cosh\beta - \cos\beta). \tag{6c}$$

PHILOSOPHICAL TRANSACTIONS OF THE ROYAL SOCIETY A MATHEMATICAL, PHYSICAL & ENGINEERING SCIENCES

The flows vary linearly with S, V, and U, and functionally with E. The solutions have very different structure depending upon whether E is large or small. If E is large, the solutions can be reduced to the following polynomials:

$$u = -(S/3!\,E)\,(z^3 - \tfrac{1}{4}z) + 2Uz, \tag{7a}$$

$$v = 2Vz, \tag{7b}$$

$$T = -\frac{S}{EP}\left(\frac{z^5}{5!} - \frac{z^3}{4!\,6} + \frac{z}{4!\,2^4}\right) + \frac{U}{P}\,(\tfrac{1}{3}z^3 - \tfrac{1}{4}z). \tag{7c}$$

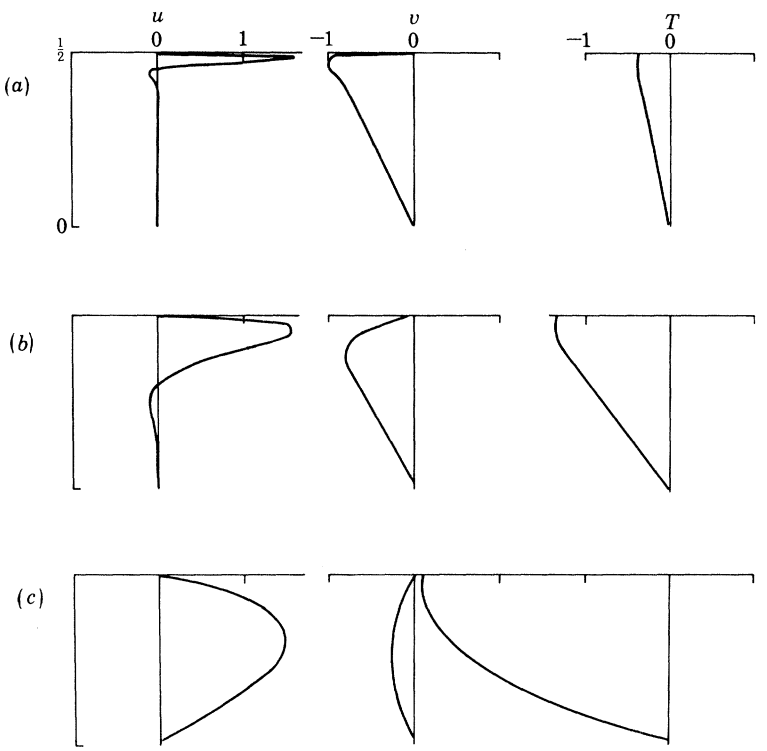

FIGURE 1. Profiles of cross-shelf velocity u, along-shelf velocity v, and temperature T as a function of $\beta = (2E)^{-\frac{1}{2}}$ for no velocity of the boundaries and $S = 1$. (a) $\beta = 64$, $E = 0.00012$; (b) $\beta = 16$, $E = 0.019$; (c) $\beta = 4$, $E = 0.03$.

The solutions for u and T are equivalent to those derived by Hansen & Rattray (1965) as model of estuarine circulation (no rotation). For E small, the solutions can be represented as Ekman layers plus interior flows because the functions (6b) and (6c) approach

$$g_1(z) \simeq \mathrm{e}^{\beta(z-\frac{1}{2})}\sin\beta(z-\tfrac{1}{2}) + \mathrm{e}^{-\beta(z+\frac{1}{2})}\sin\beta(z+\tfrac{1}{2}), \tag{8a}$$

$$g_2(z) \simeq \mathrm{e}^{\beta(z-\frac{1}{2})}\cos\beta(z-\tfrac{1}{2}) - \mathrm{e}^{-\beta(z+\frac{1}{2})}\cos\beta(z+\tfrac{1}{2}) \quad \text{for} \quad \beta \gg 1. \tag{8b}$$

For the structure of the solutions to be more clearly visualized, they were calculated by computer from equations (5) and (6) for three values of E, as shown in figure 1. Because the solutions are antisymmetric about zero, only the upper half of the solution is shown. At the top, the Ekman number is small enough for the Ekman layer to be clearly visible near the boundary. In the interior there is a linear stratification and constant shear due to the thermal wind equations (the basic state of the Eady problem). At the bottom, the Ekman number is large enough for the solution to be approaching the limit of Hansen & Rattray.

The experiment

A wide cylindrical annulus was used, rather than a very long, straight channel, to avoid problems with end walls. The tank shown in figure 2 had a Perspex bottom 1.25 cm thick and 114 cm in diameter, lying on 2 inches (*ca.* 5 cm) of insulating styrofoam. The cover could rotate with respect to the bottom tank and was covered by two inches (*ca.* 5 cm) of styrofoam. The depth of the test fluid could be held at 1, 2 or 4 cm, depending upon the height of the cover above the bottom. The inner wall of the annulus was composed of a Perspex disc of 25 cm radius, 1 cm high, upon which was mounted a waterproofed 33 Ω heating wire. Adjacent to the outer wall of the annulus was mounted a copper tube of approximately 1 cm outer diameter. This was flushed by water from a thermostatically controlled bath held at 25.3 ± 0.1 °C. Holes of diameter 2 mm were drilled down through the cover of the annulus to allow access by dye injectors and temperature probes; when not in use the holes were covered with stoppers. The entire apparatus was mounted on the 2 m turntable at Woods Hole Oceanographic Institution.

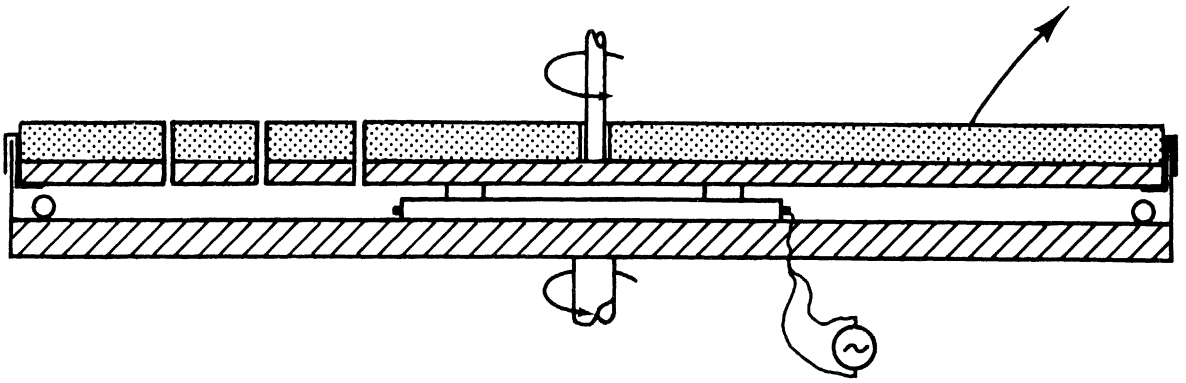

FIGURE 2. Sketch of the cylindrical experimental apparatus. The cross-hatched material is Perspex. The speckled material is styrofoam. The upper lid was free to rotate with respect to the basin. The clear area contains water.

The apparatus was like a large flattened annulus with a width:depth ratio of approximately 30:1 for a 1 cm depth, 15:1 for a 2 cm depth or 7.5:1 for a 4 cm depth. The solution of the basic flow, which was developed in the previous section, is analogous, but different from, the interior and the bottom and top boundary layers for a deep annulus as analysed by Robinson (1959). No solution is developed here for the side-wall boundary layers.

Typical measurements of temperature as a function of radius are shown in figure 3. The solid line gives the predicted profile at midplane as calculated in the next section. The temperature gradient varies with radius because the heat flux per unit area varies. This illustrates one of the most essential features of the Stommel–Leetmaa model – that temperatures at different depths parallel each other in the presence of a continuous change in temperature in the lateral direction.

The data shown here were for zero rotation but measurements at Ekman numbers down to approximately 0.02 were almost identical. However, the objection of the experiments was to observe the small Ekman number limit. They were not very successful in this respect because a time-dependent flow was almost always observed below an Ekman number of 0.02. This is most clearly shown by a series of 21 runs conducted to determine temperature between the hole of 30.4 cm radius and the hole of 50.8 cm radius as a function of rate of rotation. The results are shown in figure 4 for depths of 1 cm (solid circles) and 2 cm (open circles). The temperature

difference does not increase substantially for the 13 runs with $E > 0.02$, but for the runs with $E < 0.02$ the temperature difference began to increase, but a temporal variation was observed in the signal. The time-scales of the variations are so long that the average of the time-varying signal is not statistically well defined even after 8 h. The extremes of the temperature differences for each sample are shown in figure 4 so that the transitions to a time-dependent state could be illustrated. The values of the temperature differences were divided by a predicted value at zero rotation, which will be called ΔT_{p}, derived in the next section.

To visualize the flow, the styrofoam cover was suddenly taken off the lid and thymol blue streaks were photographed in the flowing liquid, but heat losses are so great as to render the subsequent data of only qualitative value. The time dependence comes from big eddies that slowly migrate around the tank. The eddies are usually as big as the 'shelf width'.

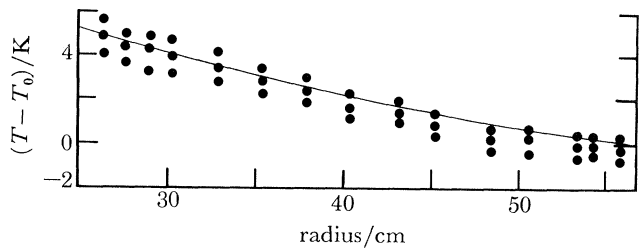

FIGURE 3. Measurements of temperature as a function of radius r at heights 1 mm (lower), 5 mm (middle), and 9 mm (upper) from the bottom of the tank. The apparatus was not rotating for these data, but data with $E = 0.3$, 0.15, 0.03 and 0.02 were almost indistinguishable from these. The solid line is a prediction of temperature dependence at the midplane of the tank.

Quantitative comparison of experiment and theory

The heat flux (Q) per unit length of shelf can be determined by the following integration:

$$Q = \int_{\frac{1}{2}}^{\frac{1}{2}} uT\,\mathrm{d}z. \tag{9}$$

In the two limits of E small and E large, the solutions (7) and (8) can be used in the integral (9) to predict the heat flux. The integrated solutions are

$$Q = -\frac{S^2}{9!\,PE^2} - \frac{4!}{9!}\frac{US}{PE} - \frac{4!}{6!}\frac{U^2}{P} \quad \text{for} \quad E \gg 0.1 \tag{10a}$$

and

$$Q = -\frac{E}{P}\left\{(\tfrac{1}{2}S+V+U)^2 - \frac{1}{2\beta}\left[3(\tfrac{1}{2}S+V)^2 + 4(\tfrac{1}{2}S+V)\,(U-U^2)\right]\right\} \quad \text{for} \quad E \ll 0.01. \tag{10b}$$

To compare the predictions with the experimental measurements of temperature as shown in figure 3, equation (10a), with $U = 0$, was put into dimensional form, the cross-shelf direction x was replaced by radius r, and the heat flux per unit radius was made equal to $H/2\pi r$.

An ordinary differential equation for T and r results, which can be integrated to give

$$T = \tfrac{3}{2}(9!\,H\nu\kappa^2/2\pi C_p\,\alpha^2 g^2 d^9\rho)^{\frac{1}{3}} r^{\frac{2}{3}} + T_0. \tag{11}$$

The parameters of the experiment were heat flux $H = 55\,\mathrm{W}$, $g = 980\,\mathrm{cm\,s^{-2}}$, specific heat

$C_p = 4.16\,\mathrm{W\,s\,g^{-1}\,K^{-1}}$, $\alpha = 3\times10^{-4}\,\mathrm{K^{-1}}$, $\nu = 0.01\,\mathrm{cm^2\,s^{-1}}$, $d = 1\,\mathrm{cm}$, $\rho = 1\,\mathrm{g\,cm^{-3}}$ and $\kappa = 0.0014\,\mathrm{cm^2\,s^{-2}}$. With these values (11) becomes

$$T - T_0 = 12.2 - 0.837 r^2_3, \tag{12}$$

where T_0 is the temperature at the outside radius (56 cm). This relation is the solid line in figure 3. The measured temperature distribution is close to that predicted although it is slightly less in the interior, possibly owing to a slight error in the thickness of the test fluid.

The temperature difference between the hole of 30.4 cm radius and the hole of 50.8 cm radius is

$$\Delta T_p = 3.31\,\mathrm{K} \quad \text{for} \quad d = 1\,\mathrm{cm},$$

and

$$\Delta T_p = 0.42\,\mathrm{K} \quad \text{for} \quad d = 2\,\mathrm{cm}.$$

These values were used to normalize the temperatures in figure 4.

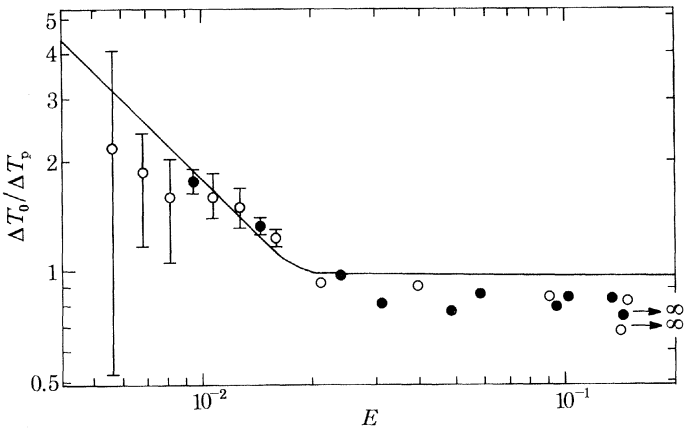

FIGURE 4. Measurements of temperature difference at the midplane between radii of 30.4 and 50.8 cm as a function of Ekman number, with constant heating voltage. The circles are means and the bars denote extremes in the measured ΔT over an eight-hour period.

Since the ratio of (10a) to (10b) is $(4/9!)^{\frac{1}{3}}E^{-3}$, and since temperature gradient scales as $H^{\frac{1}{3}}$ in (10a) and (10b), the relation $0.022E^{-1}$ (shown by the solid line in figure 4) is the solution in the small-E limit. The temperature difference was beginning to increase as E decreased in reasonably good agreement with this relation until the fluctuations became large.

Stability of the flow

We conclude that the slow-rotation limit of the theory is realizable and stable, but at high rotation an instability developed. The probable origin of the instability is suggested by the following considerations about the stability of the solution.

To estimate whether the small-Ekman-number limit is baroclinically unstable, a stability criterion derived by Pedlosky (1970, equation (3.11)) for a two-layer fluid was used with solution (5) to calculate the criterion

$$\beta\frac{E}{P}[\tfrac{1}{2}S + U + V]S\epsilon^2 < 8\left[\left(\frac{32E}{S^2\epsilon^2}\right)^{\frac{1}{2}} + \pi\right]^{-2} \tag{13}$$

for instability, where $\epsilon = d/L$. For our experiments with $U = 0$ and $V = 0$, equation (13) can be put in a more convenient form:

$$S < (4/\pi\epsilon)[(\beta Pr)^{-\frac{1}{2}} - \beta^{-1}] \tag{14}$$

for instability, where $Pr = \nu/\kappa$ is the Prandtl number.

The following values are typical of our experiment: $Pr = 5.5$, $E = 0.01$ ($\beta = 7.07$), and $\epsilon = 0.04$. These will give $S < 0.60$ for instability. Using $L\partial T/\partial x = 10\,\mathrm{K}$, $L = 25\,\mathrm{cm}$, $f = 1.0\,\mathrm{s}^{-1}$, $\alpha = 3 \times 10^{-4}\,\mathrm{K}^{-1}$, and $g = 980\,\mathrm{cm\,s}^{-2}$, we get a value of S of 0.12 which easily fits the instability criterion.

Hence it is reasonable to assume that the eddies observed here are produced by baroclinic instability. For a real shelf, with $Pr = 1$, $E = 0.01$, and $\epsilon = 0.001$, the criterion (14) (without wind stress) would be

$$S < 298.$$

Using a salinity gradient equivalent to a ΔT of 30 K, $L = 100\,\mathrm{km}$, $f = 10^{-4}$ and $\alpha = 3 \times 10^{-4}$ we get a value of S of 88, so again the criterion for instability is met.

The effect of a rotating lid

Equation (13) implies that we can stabilize the fluid by imposing differential flows in the top and bottom boundaries. This effect occurs because such differential flows do not generate vertical shear (for constant S) but do alter the stratification in the interior for the small-E limit (see equations (5*b*, *c*)). The rotating lid was incorporated to see if we could detect such an effect but it did necessitate the removal of some insulation. Of course in this experiment S will change with lid rotation anyway, so in our experiments the radial temperature gradient was measured directly by thermistors implanted in the bottom of the tank. In addition, insulation was removed from the top lid for visualization. Since heat losses were then quite large the observations of whether a flow is stable or not are only qualitative, and a quantitative verification will require a better insulated apparatus. Nonetheless a qualitative verification was obtained. Figure 5 (plate 1) shows three flows: when the lid was rotating faster than the apparatus, at the same speed, and slower. When the lid rotates faster, the flux in the Ekman layers due to differential shear is in the same sense as the buoyancy-driven flow; thus heat transport is aided, stratification is increased, and shear is decreased, resulting in a net stabilization. The dye streaks in figure 5 (*a*) are laminar except for internal waves that are radiated off the dye inserts. When the lid did not rotate differentially, the experiment was still in an unstable state as shown in figure 5 (*b*). When the lid rotated slower than the apparatus, the flux in the Ekman layers due to differential shear was opposite to the density-driven flux, i.e. water flows *toward* the centre in the top Ekman layer and *away* from the centre in the bottom one. Large shear may even force a density inversion and gravitational instability. Figure 5 (*c*) shows very strong turbulence with small eddies that rapidly mix the dye. For these runs the expression

$$\pi^2 \beta Pr\,(\tfrac{1}{2}S + V)\,S\epsilon^2,$$

which according to (13) must be less than one for instability (for $32E/S^2\epsilon^2 \ll \pi^4$), was respectively of the order of 40, 0.1, and -40. Time dependence rendered these estimates accurate to only a factor of two.

Eleven runs were made with the tank at a depth of 4 cm, and $f = 0.66\,\mathrm{s}^{-1}$, which gave an Ekman number of 9.5×10^{-4}. The velocity of the top lid was left constant for 2 hours, after which streak lines were photographed. The results were that the flow was laminar when $\pi^2 \beta Pr\,(\tfrac{1}{2}S + V) S\epsilon^2 = 10$, 7, 1.3, and 0.8; the flow exhibited large eddies like the kind in the middle of figure 5 when $\pi^2 \beta Pr\,(\tfrac{1}{2}S + V)\,S\epsilon^2 = -2$, -5, and -40.

In view of the uncertainty about the estimates of lateral density gradient, it appears that the main prediction of the theory – that the flows are subjected to baroclinic instabilities or actual

PHILOSOPHICAL TRANSACTIONS OF THE ROYAL SOCIETY A MATHEMATICAL, PHYSICAL & ENGINEERING SCIENCES

density inversions when certain critical parameters are exceeded – has been verified. Although it is tempting to report more quantitative details, the effect of heat loss, depth variation up to 1 mm, and influence of the measuring probes may dominate them.

On real shelves (which might have a density flux due to fresh water run off rather than heat) we note that winds would aid the flux of low density water offshore, as does our prograde rotating lid, if they are blowing offshore or to the left facing offshore (in the Northern Hemisphere and on the assumption that low density water is near the coast). Those winds would tend to stabilize the flow. When winds blow onshore or to the right the density flux would be hindered and the waters would be destabilized as in figure 5(*c*).

The effects of a free boundary

If there is a stress-free boundary above the water for small Ekman number, the Ekman layer is changed to a zero-stress Ekman layer. This layer transforms the uniform vertical shear generated by the thermal wind relation to zero and is not capable of advecting as much heat laterally. The solutions of equations (2*a–d*) in the limit of small E, with the boundary conditions

$$\partial u/\partial z = \partial v/\partial z = \partial T/\partial z = 0 \quad \text{at} \quad z = \tfrac{1}{2},$$
$$u = v = \partial T/\partial z = 0 \quad \text{at} \quad z = -\tfrac{1}{2},$$

have the form

$$u = -(S/2\beta)\,\mathrm{e}^{\beta(z-\frac{1}{2})}[\sin\beta(z-\tfrac{1}{2}) - \cos\beta(z-\tfrac{1}{2})] - (S/\beta)\sin\beta(z+\tfrac{1}{2})\,\mathrm{e}^{-\beta(z+\frac{1}{2})}, \tag{15a}$$

$$v = (S/2\beta)\,\mathrm{e}^{\beta(z-\frac{1}{2})}[\sin\beta(z-\tfrac{1}{2}) + \cos\beta(z-\tfrac{1}{2})] - (S/\beta)\cos\beta(z+\tfrac{1}{2})\,\mathrm{e}^{-\beta(z+\frac{1}{2})} - S(z+\tfrac{1}{2}) + S/\beta, \tag{15b}$$

$$T = (ES/2P\beta)\,\mathrm{e}^{\beta(z-\frac{1}{2})}[\sin\beta(z-\tfrac{1}{2}) + \cos\beta(z-\tfrac{1}{2})] - (ES/P\beta)\cos\beta(z+\tfrac{1}{2})\,\mathrm{e}^{-\beta(z+\frac{1}{2})} - (ES/P)(z). \tag{15c}$$

This solution differs from the rigid-lid solutions in two ways. First, heat flux per unit temperature gradient is decreased by a factor of β^{-1} owing to the presence of that factor in (15*a*). Secondly, a net transport along the shelf (around the annulus) is predicted in (15*b*). To test whether transport is observed, the rigid lid was removed from the tank, and the temperature of the bath was set at 5 °C so that the water in the apparatus would remain cold and would not transfer much heat to the atmosphere. The basin was covered with clear cellophane. The voltage of the heater was set at 30 V a.c., so that an r.m.s. wattage of 13.5 W was produced. The apparatus was rotated until the temperature field of the liquid built up to a steady value, after which dye was injected into the fluid. Photographs of the dye streaks were taken every 5 s to record movement of the dye, and a steady flow around the cylindrical tank was observed.

One can predict velocity as a function of heat flux by using solutions (15*a–c*) to predict $\partial T/\partial x$ as a function of heat flux:

$$\partial T/\partial x = (8f^3H\beta/d^3\rho C_p g^2\alpha^2 Pr)^{\frac{1}{3}},$$

where H is heat flux per unit length of shelf, C_p is the specific heat, and α is the coefficient of expansion. The velocity as a function of heat production per centimetre of arc is

$$v = 2(g\alpha H/\rho C_p Pr)^{\frac{1}{3}}(2E)^{-\frac{1}{6}}.$$

For the experiment, the appropriate magnitudes are $g = 980\,\mathrm{cm\,s^{-2}}$, $\rho C_p = 4.16\,\mathrm{W\,s\,K^{-1}\,cm^{-3}}$, $\alpha = 3\times10^{-4}$, $H = 0.09\,\mathrm{W\,cm^{-1}}$, and $Pr = 5.5$, and so the velocity as a function of E is given by

$$v = 0.20(2E)^{-\frac{1}{6}}.$$

For this experiment $E = 0.311\times10^{-2}$, and the above E-formula gives a velocity of $0.48\,\mathrm{cm\,s^{-1}}$;

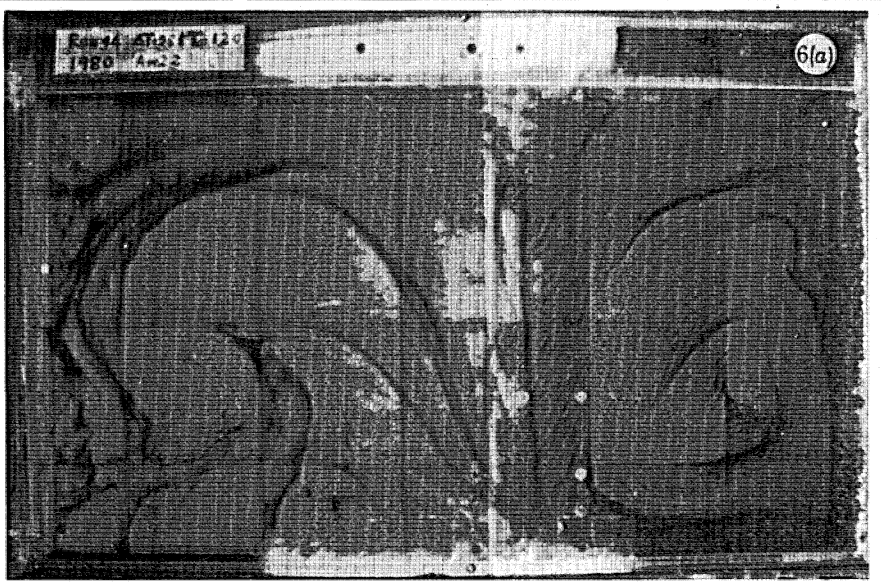

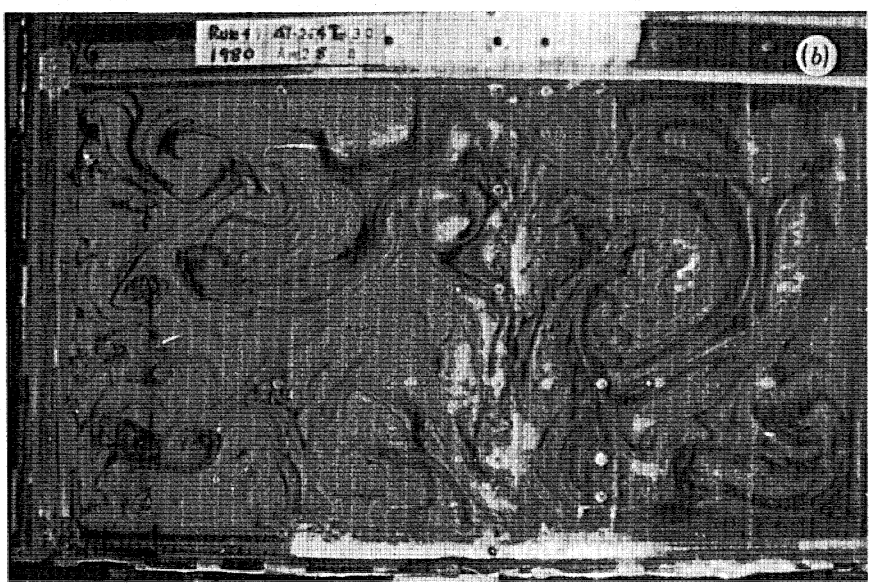

FIGURE 5. Streak lines for the first experiment when the upper lid is rotating (*a*) faster than the tank, (*b*) with the tank and (*c*) slightly slower than the tank. The streak lines on the left are wavy owing to internal lee waves being scattered off the dye probe; otherwise the flow is laminar. The streak lines on the middle reveal large sluggish eddies. On the right the differential shear of the lid is generating a very small stratification that has considerable small-scale turbulence which mixes the dye. The Ekman number is 9.5×10^{-4}.

FIGURE 6. (*a*) Streak lines for moderate rotation. The dark dye comes off wires that are strung across the tank. (*b*) Streak lines for fast rotation. The geostrophic eddies are visible throughout the shelf, some with sinking regions.

(*Facing p.* 590)

PHILOSOPHICAL TRANSACTIONS OF THE ROYAL SOCIETY A MATHEMATICAL, PHYSICAL & ENGINEERING SCIENCES

the velocity of the dye was about the same. Other runs were done at different rates of rotation, and observed velocities did appear to agree crudely with computed velocities, but there were sufficient heat losses and wind drag to discourage attempts to obtain precise quantitative comparisons.

In summary, even this simplest shelf model can often be unstable. Winds can affect the model by generating circulations that will either increase or decrease heat (or fresh water) transport and thereby alter the stability. Alongshore currents can be generated as predicted.

2. A shallow sea with dense water formation

If waters in a shallow sea are subjected to much surface cooling and evaporation, they are found to be denser than water in the neighbouring deep ocean. This is due to the effect of surface-evaporative and sensible cooling, both of which decrease temperature, and the first of which increases salinity also. Often this denser water stays confined on the shelf owing to the action of wind set-up or because of topographic barriers. Sometimes the water is observed to spill off the edge of the shelf and irreversibly contribute to the deep waters of the world's oceans. An outstanding and important example of this later class of shelf flows is the flow off the shelf of the Weddell Sea, as discussed by Gill (1973) and Killworth (1979). A recent observation by Foldvic (private communication) of a strong bottom current coming off the Weddell Sea through the Filchner depression emphasizes the importance of shelf regions in generating the thermohaline structure of the oceans.

The main part of the second experiment (built by T. Sugimoto, who also did the bulk of this experiment in consultation with the author) was a rectangular basin mounted on a rotating turntable. In the basin is a square shelf 50 cm × 50 cm × 5 cm deep connected by a narrow (10 cm wide) slope to a deeper basin 30 cm × 50 cm × 15 cm deep. The slope thus emphasizes the dramatic contrast between shelf (which in our model has zero bottom slope even though real shelves do not) and shelf break. The enclosed fluid is cooled through a top lid and heated through an offshore aluminum side wall. This experiment thus also emphasizes winter, or intense evaporation, rather than summer or fresh-water run-off which was emphasized in § 1. Outside the wall is a stirred thermostatically regulated bath. The bottom of the top lid is composed of Perspex plate 6 mm thick above which is a channel 6 mm deep, 56 cm wide, and 91 cm long, through which chilled water is made to flow. The channel is covered above by a 6 mm Perspex plate. Running water is introduced at one end of the lid and removed at the other end, the water coming from a cooled thermostatically controlled bath. The temperature difference between the test fluid and the water in the upper lid was much larger than temperature variation in the tank, so to a first approximation the fluid was cooled uniformly from above. Side walls and the bottom of the test chamber were made of Perspex plate 12.6 mm thick for better insulation.

Photographs of the current pattern were taken by a 35 mm camera and also by a 16 mm ciné camera 1.1 m above the top of the basin. Visualization was with the thymol blue method in which a pH-sensitive indicator is buffered to its transition pH, so that an electric voltage applied between wires results in the fluid near the wires changing from yellow to dark blue. It was possible to trace the movement of the fluid for a few minutes thereafter. Temperature in the basin was measured by a thermistor put through one of 25 small holes in the top lid.

It took over 3 h for the temperature distribution of the test fluid to become steady. Although the current patterns change almost continuously with rate of rotation, they can be classified into the following three groups.

PHILOSOPHICAL TRANSACTIONS OF THE ROYAL SOCIETY A MATHEMATICAL, PHYSICAL & ENGINEERING SCIENCES

(*a*) Very slow or no rotation. The tank is smaller than the Rossby radius ($[g(\partial\rho/\rho\partial z)\,d^2]^{\frac{1}{2}}f^{-1}$). Vertical circulations predominante so that flow is like a Hadley cell. Water is heated at the offshore wall and flows toward the inner shelf, bending slightly to its right (for anticlockwise tank rotation). The heated water is also being cooled from above so there is a surface-mixed layer with convection rolls aligned in the direction of flow. In the 'sinking' region the mixed layer extends to the bottom. The densest water in the tank is in this region, and it sinks under the surrounding water, makes its way to the shelf break (curving to the right) and plunges off the edge of the shelf break to form bottom water in the model 'ocean'. The sinking region is limited to a narrow inner coastal zone, the width of the zone being less than 2 cm.

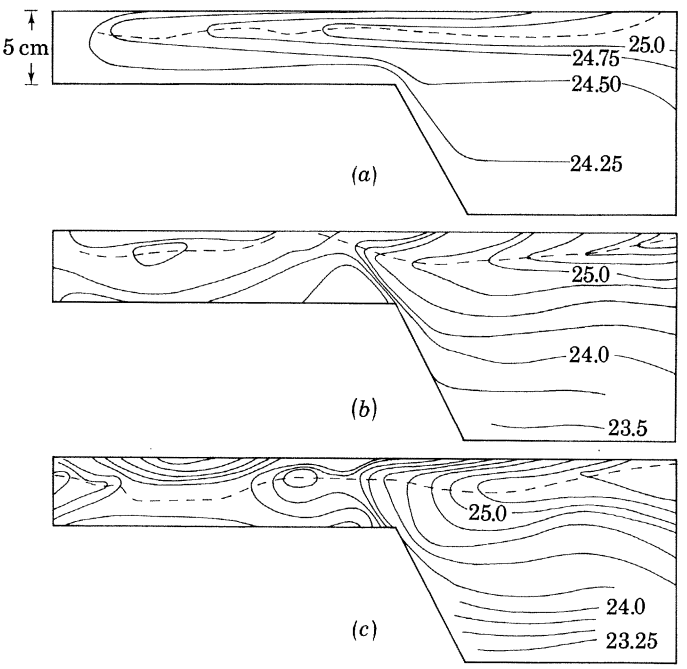

FIGURE 7. A temperature section from shelf to shore for (*a*) no rotation, (*b*) moderate rotation, and (*c*) fast rotation.

(*b*) Moderate rotation (figure 6*a*, plate 1). The tank is approximately the size of the Rossby radius. Horizontal single gyres of basin scale are formed on the shelf. The flow of hot water into the shelf is cyclonic and the lower outflow from the sinking region is anticyclonic. The sinking region is in the right-hand corner (facing offshore). Cold water formed there flows along the shelf break, curving toward the right, hits the right-hand wall and spills off from the shelf in a strong downwelling jet. As the rotation rate is increased, the width of the jet decreases, and curvature of the gyre increases. Also the gyre tends to retreat toward the inner coastal part of the shelf.

(*c*) Strong rotation (figure 6*b*, plate 1). The tank is larger than the Rossby radius. Turbulent eddies are predominant: they fill the shelf as well as the offshore region. Sinking occurs in the centre of some, but not all, eddies. The eddies are mostly cyclonic in the upper layer and anticyclonic in the lower layer but occasionally a gyre is cyclonic from top to bottom. The size of the eddies decreases as the rotation rate is increased. On average the shelf-bottom water flows slowly along the shelf break towards the right-hand side-wall (facing offshore) and flushes out as a downwelling jet at the right-hand wall, but cyclonic eddies on the shelf break also contribute to

PHILOSOPHICAL TRANSACTIONS OF THE ROYAL SOCIETY A MATHEMATICAL, PHYSICAL & ENGINEERING SCIENCES

the flushing of the shelf water. Warm surface water offshore enters onto the shelf intermittently in the upper layer above the shelf break as well as along the left-hand side-wall (facing offshore).

The transition from (*b*) to (*c*) is variable. Sometimes two, three or four gyres are steady, at other times the fluid is very unsteady.

Thermal structures

(*a*) Slow or zero rotation (figure 7*a*). Thermal effluents about 2.5 cm thick extend from the offshore side-wall towards the shelf. They are cooled down rapidly but intrude close to the inner coastal-wall boundary of the shelf by advection. Upper layers are well mixed (convection rolls were clear) but the lower layer is stratified.

(*b*) Moderate rotation (figure 7*b*). Warm offshore water comes into the shelf along both the right-hand and left-hand side-wall boundaries and then circulates. The density structure is basically the same as that for (*a*) except that the width of the density current along the walls decreases. There is a strong jet flowing along the shelf break towards the right-hand side in the lower layer. It hits the right-hand wall (facing offshore) and cascades down the slope.

(*c*) Fast rotation (figure 7*c*). Temporal variability is significant owing to turbulent eddies, and each vertical section differs. However, usually a distinct thermal front is formed at the shelf break, although the front wanders around and varies in association with turbulent eddies.

This experiment, although extremely complicated physically, points out phenomena that may exist on real shelves in winter (or on shelves subjected to intense evaporation). Measurements of the curvature of the circulations on the shelf indicate that the radius of the gyres is roughly proportional to the internal Rossby radius of deformation NH/f, where H is the depth of the shelf and N is the local Brunt–Väisälä frequency. Also, a sizeable percentage of the flux off the shelf occurs near the right-hand wall, through a rotating density current. The magnitude of the temperature difference between the sinking and offshore regions can be reasonably predicted through the use of simple rotating hydraulic formulas (as given in Whitehead *et al.* 1974) of the form $Q = g^* h^2/2f$, where h is the fluid depth of the entire shelf and Q is volumetric flux. Equating $g^* = g\alpha\Delta T$ and $H = \rho C_p \Delta T Q$, where ΔT is the temperature difference between the coldest water and the water offshore, we predict $\Delta T = (2fH/\rho C_p \alpha g h^2)^{\frac{1}{2}}$. This formula was reasonably well obeyed. There is usually a distinct front at the edge of the shelf which hinders sizeable mass flux off the span of the shelf break. It is not known why this front is so persistent. Finally, the sinking regions are only located in a predictable region for small rotation rates (large Rossby radius compared with the shelf). For larger rotation rates the sinking regions must first be located by some remote sensing method. In the laboratory a human eye often suffices but in the real ocean spaceborne or airborne sensors may have to be used. Finally, the elusive chimneys (Killworth 1979) may have been observed here. The general nature of our sinking regions – cyclonic inflow to a sinking region with one or more sinking plumes, and anticyclonic outflow from the water formation region, seems to be similar. By forcing the water to have a convection region we may have produced what may happen not only on shelves but also in deep polar oceans.

3. Rotating gravity current

The third laboratory models were done in conjunction with M. Stern, B. L. Hua & N. Paldor (manuscript in preparation). The purpose was to model a gravity current in a rotating fluid. The work was primarily motivated by a recent theory by Stern (1980) and by the possibility that

PHILOSOPHICAL TRANSACTIONS OF THE ROYAL SOCIETY A MATHEMATICAL, PHYSICAL & ENGINEERING SCIENCES

inertial jets lie along the coasts of some shelves, generated by intense spring run-off or large density contrasts near straits.

Experiments were made in a Plexiglass rectangular tank. Grooves were cut into the sides and bottom of the tank to allow a sliding gate, of 22-gauge (0.80 mm) stainless steel, to divide the tank into two chambers. The procedure was to fill the tank with tap water to a depth of 18.7 cm. A measured amount of salt was added to the water, and the water was mixed thoroughly. The gate was slid into the set of slits to a depth 10 cm above the bottom of the tank, and two pieces of $\frac{1}{4}$ inch (or *ca.* 0.6 cm) plywood were floated in the shorter chamber on one side of the gate. The tank was covered by a Plexiglass lid, the turntable was brought to the desired rate of rotation, and the salt water was allowed to spin for 15 min to reach a state close to solid-body rotation. The preparation for the experiment was completed by siphoning some coloured water onto the plywood floats in the small chamber until 4 cm of fresh water floated above the salty water.

After the gate was removed, the fresh water was observed to flow over the salt water, and the Coriolis force caused the water to flow as a geostrophic gravity current towards the 'coast' (the right-hand wall looking downstream with the basin rotating counterclockwise). The current was then deflected by the wall and caused to flow downstream next to that wall. The current is similar to a non-rotating density current in that it has a front deeper than the *current* behind, and was observed to move with speed of approximately $1.6(g^*h)^{\frac{1}{2}}$, where $g^* = g\delta\rho/\rho$, $\delta\rho$ is the density difference between the two fluids, and h is the local depth. It differs from its non-rotating counterpart in several ways. The most obvious is that it hugs the right-hand wall. It has a width of approximately $0.4(g^*h')^{\frac{1}{2}}f^{-1}$. It detrains eddies laterally rather than vertically; these eddies lie alongside the more laminar current.

It is anticipated that such currents may be encountered near the mouths of rivers or near straits connecting bodies of water of different densities, in which case measurements of propagation speed and width would be interesting. The observation of a possible gravity current by Mork (this symposium) is promising.

4. Concluding remarks

Very shallow shelves (§ 1), shelves with a strong break and sides (§ 2), and coastal jets (§ 3) have been described in this paper. All experiments demonstrated the tendency for baroclinic processes on shelves to form geostrophic turbulence. In the first experiment the cross-shelf density flux was provided by viscous boundary layers. In the second and third by a side-wall. In shallow seas the flushing may be aided or hindered by winds, bathymetry, tides, offshore pressure gradients or other factors, but clearly the role of the eddies must often be addressed. This is one of the challenges for future laboratory studies.

We have purposely not applied these models in detail to specific shelves nor have we hoped to cover comprehensively all the types of shelves in the world. Since there are at least 150 000 km of shelves in the world it is reasonable to expect that there are some shelves modelled well by these few examples, while others (possibly most) are not. A realistic assessment and hints for other models will come as the oceanography of shallow seas matures.

Support for this research was from the Ocean Sciences Division, National Science Foundation, under Grant OCE80-18322 for the first two experiments, and the United States Office of Naval Research for the third under contract N00014-81-C-0010. Thanks are due to T. Sugimoto for allowing the use of his data and to Robert Frazel for skilful laboratory assistance.

PHILOSOPHICAL TRANSACTIONS OF THE ROYAL SOCIETY A MATHEMATICAL, PHYSICAL & ENGINEERING SCIENCES

References (Whitehead)

Beardsley, R. C. & Festa, J. F. 1972 *J. phys. Oceanogr.* **2**, 444–455.
Brocard, D. N., Jirka, G. H. & Harlemann, R. E. D. 1977 Technical Report 223, Dept of Civil Engineering, Massachusetts Institute of Technology.
Csanady, G. T. 1976 *J. geophys. Res.* **81**, 5389–5399.
Gill, A. E. 1973 *Deep Sea Res.* **20**, 111–140.
Hansen, D. V. & Rattray, M. 1965 *J. mar. Res.* **23**, 104–122.
Killworth, P. D. 1979 *J. phys. Oceanogr.* **9**, 531–554.
Pedlosky, J. 1970 *J. atmos. Res.* **27**, 15–30.
Phillips, O. M. 1966 *Deep Sea Res.* **13**, 1149–1160.
Robinson, A. R. 1959 *J. Fluid Mech.* **6**, 599–620.
Scott, J. T. & Csanady, G. T. 1976 *J. geophys. Res.* **81**, 5401–5409.
Stern, M. E. 1980 *J. Fluid Mech.* **99**, 687–704.
Stommel, H. 1962 *Proc. natn. Acad. Sci. U.S.A.* **48**, 766–772.
Stommel, H. & Leetmaa, A. 1972 *Proc. natn. Acad. Sci. U.S.A.* **69**, 3380–3384.
Taylor, G. I. 1953 *Proc. R. Soc. Lond.* A **219**, 446–468.
Whitehead, J. A., Leetmaa, A. & Knox, R. A. 1974 *Geophys. Fluid Dyn.* **6**, 101–125.

PHILOSOPHICAL TRANSACTIONS OF THE ROYAL SOCIETY A MATHEMATICAL, PHYSICAL & ENGINEERING SCIENCES

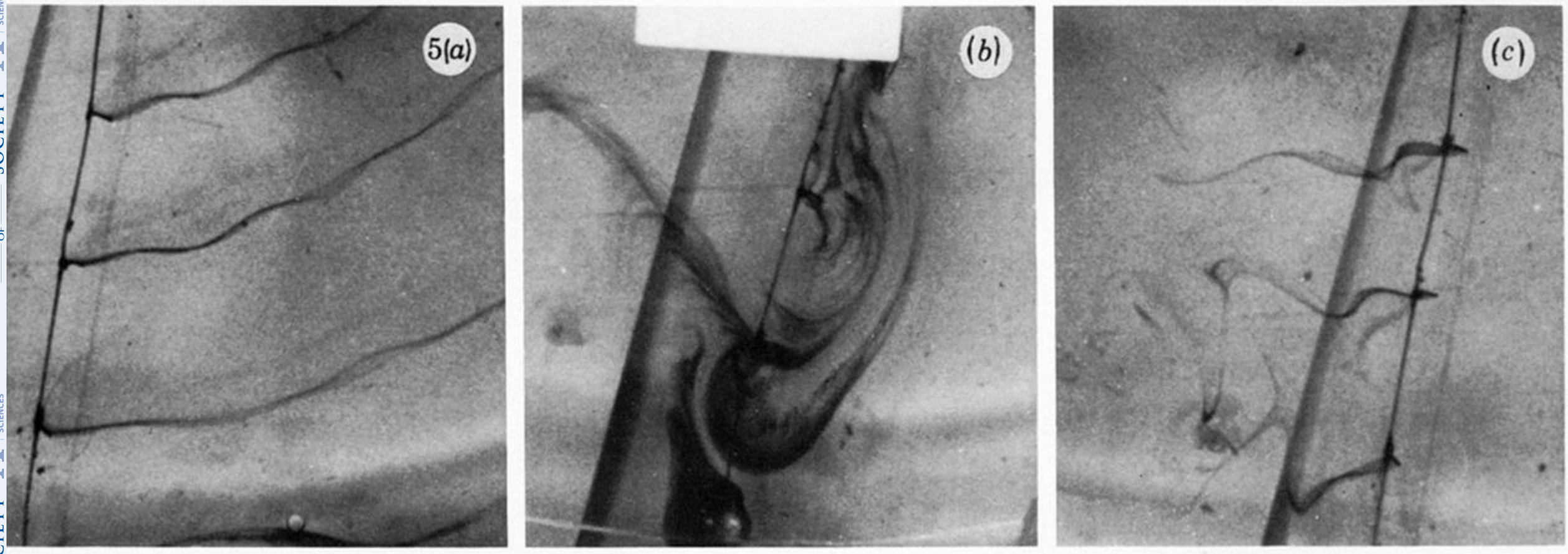

FIGURE 5. Streak lines for the first experiment when the upper lid is rotating (*a*) faster than the tank, (*b*) with the tank and (*c*) slightly slower than the tank. The streak lines on the left are wavy owing to internal lee waves being scattered off the dye probe; otherwise the flow is laminar. The streak lines on the middle reveal large sluggish eddies. On the right the differential shear of the lid is generating a very small stratification that has considerable small-scale turbulence which mixes the dye. The Ekman number is 9.5×10^{-4}.

PHILOSOPHICAL TRANSACTIONS OF THE ROYAL SOCIETY A MATHEMATICAL, PHYSICAL & ENGINEERING SCIENCES

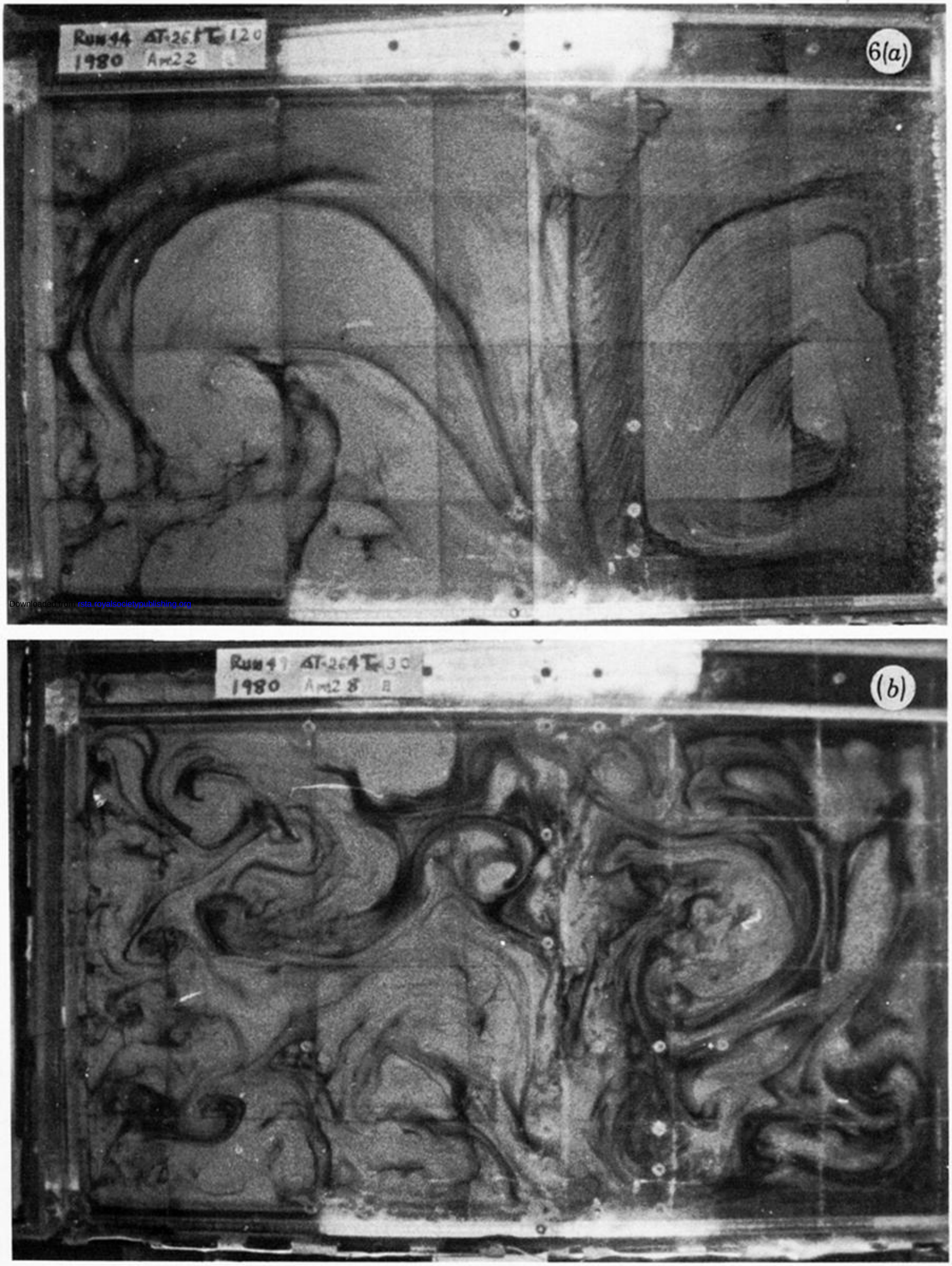

FIGURE 6. (*a*) Streak lines for moderate rotation. The dark dye comes off wires that are strung across the tank. (*b*) Streak lines for fast rotation. The geostrophic eddies are visible throughout the sheif, some with sinking regions.